EINDHOVEN UNIVERSITY OF TECHNOLOGY

Influence of the tip work function on scanning tunneling microscopy and spectroscopy on zinc doped GaAs

Citation for published version (APA):
Wijnheijmer, A. P., Garleff, J. K., van der Heijden, M. A., & Koenraad, P. M. (2010). Influence of the tip work function on scanning tunneling microscopy and spectroscopy on zinc doped GaAs. *Journal of Vacuum Science and Technology B*, *28*(6), 1086-1/7. https://doi.org/10.1116/1.3498739

DOI:
10.1116/1.3498739

Document status and date:
Published: 01/01/2010

Document Version:
Publisher's PDF, also known as Version of Record (includes final page, issue and volume numbers)

Please check the document version of this publication:

• A submitted manuscript is the version of the article upon submission and before peer-review. There can be important differences between the submitted version and the official published version of record. People interested in the research are advised to contact the author for the final version of the publication, or visit the DOI to the publisher's website.
• The final author version and the galley proof are versions of the publication after peer review.
• The final published version features the final layout of the paper including the volume, issue and page numbers.

Link to publication

General rights
Copyright and moral rights for the publications made accessible in the public portal are retained by the authors and/or other copyright owners and it is a condition of accessing publications that users recognise and abide by the legal requirements associated with these rights.

• Users may download and print one copy of any publication from the public portal for the purpose of private study or research.
• You may not further distribute the material or use it for any profit-making activity or commercial gain
• You may freely distribute the URL identifying the publication in the public portal.

If the publication is distributed under the terms of Article 25fa of the Dutch Copyright Act, indicated by the "Taverne" license above, please follow below link for the End User Agreement:

www.tue.nl/taverne

Take down policy
If you believe that this document breaches copyright please contact us at:

openaccess@tue.nl

providing details and we will investigate your claim.

Download date: 16. Nov. 2023

Influence of the tip work function on scanning tunneling microscopy and spectroscopy on zinc doped GaAs

A. P. Wijnheijmer,[a)] J. K. Garleff, M. A. v. d. Heijden, and P. M. Koenraad
COBRA Inter-University Research Institute, Department of Applied Physics, Eindhoven University of Technology, P. O. Box 513, NL-5600 MB Eindhoven, The Netherlands

(Received 17 May 2010; accepted 13 September 2010; published 12 October 2010)

The authors investigated the influence of the tip work function on the signatures of zinc in gallium arsenide with scanning tunneling microscopy and spectroscopy. By deliberately inducing tip modifications, the authors can change the tip work function between 3.9 and 5.5 eV, which corresponds to the expected range for tungsten of 3.5–6 eV. The related change in flatband voltage has a drastic effect on both the dI/dV spectra and on the voltage where the typical triangular contrast appears in the topography images. The authors propose a model to explain the differences in the dI/dV spectra for the different tip work functions. By linking the topography images to the spectroscopy data, the authors confirm the generally believed idea that the triangles appear when tunneling into the conduction band is mainly suppressed. © *2010 American Vacuum Society.*
[DOI: 10.1116/1.3498739]

I. INTRODUCTION

Shallow and deep acceptors in III-V semiconductors have been the subject of many scanning tunneling microscopy (STM) studies in recent years. Both shallow and deep acceptors have a by now familiar anisotropic shape, which was first reported for the shallow acceptor Zn in GaAs in 1994 (Refs. 1 and 2) and for the deep acceptor Mn in GaAs in 2004.[3] Since then, many authors have studied these acceptors with STM.[4–14] All the STM studies report that the anisotropic contrasts appear at small positive sample voltages, but the specific voltage differs between 0.6 V (Ref. 3) and up to 3 V.[1,2] Furthermore, it is commonly accepted by now that the anisotropic contrast appears at different voltages from tip to tip on the same sample. It is generally believed that the anisotropic shape is visible when tunneling into the conduction band is suppressed. There is still a debate, however, about the exact nature of the triangular shape of the shallow acceptors [see, e.g., Figs. 1(c) and 1(e)] or the bow-tie-like shape for deep acceptors. For example, the authors in Ref. 4 suggest that the triangle appears due to tunneling into the empty valence band (VB) states, implying that tunneling into the conduction band (CB) is completely suppressed. Reference 6 states that the triangles are only visible when there is a depletion layer underneath the tip and proposes a model that involves resonant tunneling through evanescent gap states.[8] Other authors suggest that the triangle appears due to tunneling into the excited state of the acceptor.[12] In the case of the deep acceptor Mn in both InAs and GaAs, it is generally believed that the wave function is imaged,[7,9,11,13,14] where mixing between spherical harmonic functions with *s* and *d* characters are responsible for the bow-tie shape. Furthermore, it was shown recently that the symmetry is lifted for acceptors close to the surface due to surface induced strain.[9]

[a)]Electronic mail: a.p.wijnheijmer@tue.nl

In this study, we investigate the influence of the tip work function on the Zn signatures in STM and scanning tunneling spectroscopy (STS). We deliberately change the tip work function and experimentally extract the tip work function. The extraction of the tip work function is based on the method proposed by Loth *et al.*,[6] which we elaborate by including the effect of image charges. We observe two qualitatively different situations in the STS data, depending on the tip work function. Hardly any zinc-induced peaks in the dI/dV spectra are visible in the first case, whereas in the second case strong peaks are present at the Zn atoms, which are followed by negative differential conductivity.

We start the article by briefly discussing the experimental technique, followed by our results. We then describe the method of extracting the flatband voltage experimentally in detail, which is necessary for the analyses and interpretation of our results given in the final section of the article.

II. EXPERIMENT

We performed cross-sectional STM and STS at 5 K on Zn-doped GaAs, with an average doping concentration of 2×10^{19} cm^{-3}. We cleaved our samples in UHV with a base pressure of 10^{-11} mbar to obtain a clean and atomically flat {110} surface. We used chemically etched polycrystalline tungsten tips. Further preparation in UHV (Ref. 15) guaranteed sharp tips with atomic resolution and stability over days in STS mode at low temperatures.

III. RESULTS

Figure 1 shows a series of STM topography images, measured at different sample voltages and with two different tips. We see the same behavior in the STM images as is presented in Refs. 4–6 and 12. At a high positive sample voltage [Fig. 1(a)], the Zn atoms appear as dark depressions; at lower positive voltages [Fig. 1(b)], bright features start to appear but the depressions are still visible; and at an even

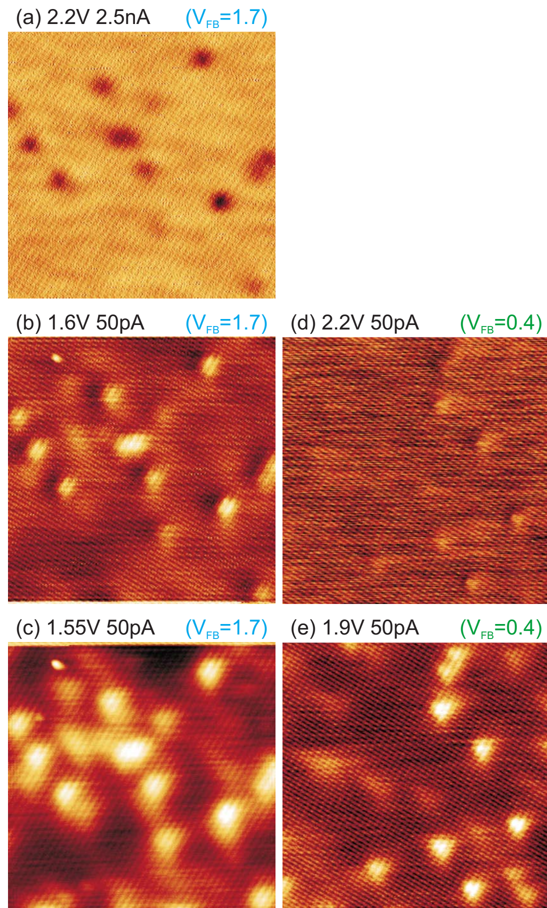

FIG. 1. (Color online) Series of topography images of Zn-GaAs at different voltages. (a)–(c) are measured with the same tip, while (d) and (e) are measured with a different tip. External voltage, current setpoint, and flatband voltage V_{FB} are indicated. The images are 25×25 nm^2. The typical triangular contrast appears at low positive voltages. This $V_{\triangleright}$ strongly depends on the flatband voltage.

lower voltage [Fig. 1(c)], the typical triangular features appear. This behavior is similar for all the positive bias STM images of Zn–GaAs. The triangles appear at a well defined voltage, as can be seen in Figs. 1(b) and 1(c). The voltage difference between the two images is only 50 mV, but in Fig. 1(b) there are still dark depressions visible near the tip of the triangle that are gone in Fig. 1(c). It is important to note that the triangles remain visible when reducing the sample voltage. Therefore, we define $V_{\triangleright}$ as the highest voltage where the bright triangles can be observed without any visible depressions in topography images. Although the behavior is similar in all the measurements, $V_{\triangleright}$ differs for different tips. This is clearly visible in Figs. 1(c) and 1(e), which were measured with different tips. In both images the triangles are clearly visible, but they are measured at voltages that differ by 0.35 V.

IV. EXTRACTING THE FLATBAND VOLTAGE

In order to understand the origin of the differences in $V_{\triangleright}$, we deliberately induced tip modifications, measured $V_{\triangleright}$, and determined the tip work function Φ_{tip} for each tip. For the determination of Φ_{tip}, we followed the procedure as described in Ref. 6 and improved it for our measurement. We first give a very short description of the principle of the method.

This method is based on measuring an $I(z_t)$ spectrum by changing the tip-sample distance (z_t) and measuring the current (I). In our case, we change I and measure z_t, because it turned out to be more reliable. An example of such a measurement is shown in Fig. 2. In approximation, the tunneling current depends exponentially on the tip-sample distance, $I\propto\exp(-2\kappa z_t)$, thus, $\kappa=\ln(I_1/I_2)/(2(z_{t,2}-z_{t,1}))$. κ is the inverse decay length, which can be transformed into an effective barrier height Φ_B using $\kappa=\sqrt{2m_0\Phi_B}/\hbar$. Loth *et al.*[6] neglected the effect of image charges and approximated the tunneling barrier by a trapezium. They subsequently translated the effective barrier height into the tip work function, where they used geometrical arguments

$$\mathrm{eV}<E_g:\quad \Phi_{tip}=2\Phi_B-\chi-E_g-\mathrm{eV}+|\mathrm{TIBB}|, \tag{1a}$$

$$\mathrm{eV}>E_g:\quad \Phi_{tip}=2\Phi_B-\chi-E_g+\mathrm{eV}-\mathrm{TIBB}. \tag{1b}$$

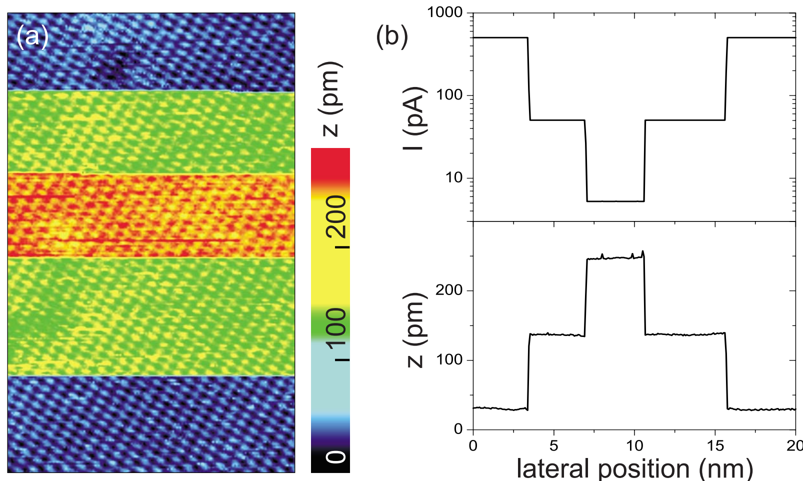

FIG. 2. (Color online) (a) Topography image measured at 2.4 V, where we varied the current setpoint. The current was 500 pA in the blue areas, 50 pA in the green areas, and 5 pA in the yellow-red area. (b) Cross sections through the image shown in (a) and the corresponding current image, averaged over the whole width of the image, showing the changes in the current setpoint and the corresponding changes in the tip-sample distance.

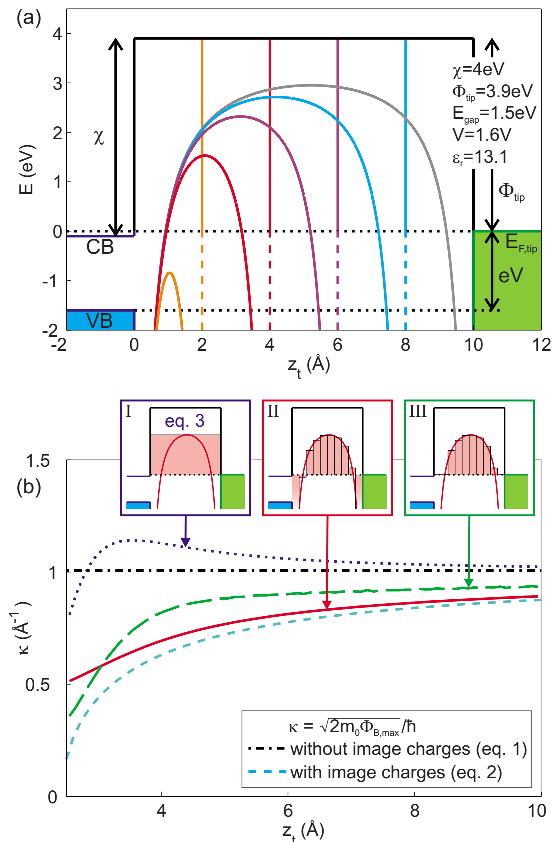

FIG. 3. (Color online) (a) Reduction of the tunneling barrier due to the effect of image charges. The barriers are shown on scale. Various parameters are indicated. (b) Comparison between the decay length κ as found with various approximations. See the text for details.

We use the bulk values of 4.07 eV and 1.519 eV for the electron affinity χ and the band gap energy E_g, respectively. The tip induced band bending (TIBB) is calculated by the model developed by Ref. 16.

In our analysis, we include two effects that Loth *et al.*[6] neglected. They turn out to have a significant effect. The first is the effect of the image charges due to the tunneling electron. Second, we use a more advanced approximation for the dependence of the tunneling current on the tip-sample distance than the commonly used approximation $I \propto \exp(-2\kappa z_t)$.

We first discuss the effect of the image charges due to the tunneling electron. The reduction of the tunneling barrier due to image charges has been studied extensively in the literature.[17–19] We consider a semi-infinite metal (the tip) on top of a semi-infinite semiconductor slab with a dielectric constant ϵ_r, separated by a vacuum barrier with a width z_t. The potential due to the image charges is then given by Eq. (2) as follows:[17–19]

$$\Phi_i = -\frac{e^2}{8\pi\epsilon_0}\left[\frac{1}{2z} + \sum_{n=1}^{\infty}\left(\frac{(1/2)a^n}{z_t n + z} + \frac{(1/2)a^n}{z_t n - z} + \frac{a^n}{z_t n}\right)\right], \quad (2)$$

where $a=(\epsilon_r - 1/\epsilon_r + 1)$. This barrier is shown on scale in Fig. 3(a) for various tip-sample distances (z_t), where we use an electron affinity of the sample χ of 4 eV, a tip work function Φ_{tip} of 3.9 eV, and a sample voltage of 1.6 V. The CB, VB, and Fermi level of the tip ($E_{F,tip}$) are indicated. The image charges clearly cause a strong reduction of the effective tunneling barrier. The smaller the tip-sample distance, the bigger the effect. For $z_t \lesssim 2.5$ Å, the barrier even becomes negative. In Fig. 3(b), the corresponding reduction in κ is plotted, where we calculated κ at the maximum of the barrier $\kappa = \sqrt{2m_0\Phi_{B,max}}/\hbar$ (WKB approach, see, for example, Ref. 20). The dashed-dotted black line corresponds to the original rectangular barrier and the short-dashed cyan line corresponds to the barrier including the image charge potential.

The second effect is a bit more subtle. The key element is that the approximation of the tunneling current in STM analyses by $I \propto \exp(-2\kappa z_t)$ is not accurate for $z_t \lesssim 5$ Å. This effect is described in detail in, for example, Ref. 21. The full expression for tunneling through a rectangular barrier is given by[20]

$$I \propto \frac{4\tilde{k}_t\tilde{k}_s\kappa^2}{\kappa^2(\tilde{k}_t^2 + \tilde{k}_s^2) + (\tilde{k}_t^2 + \kappa^2)(\tilde{k}_s^2 + \kappa^2)\sinh^2(\kappa z_t)}. \quad (3)$$

Here, $\tilde{k}_{t,s}$ are the wave vectors in the tip and the sample, respectively, divided by their effective masses. κ is the inverse decay length, defined by $\kappa \equiv \sqrt{2m_0\Phi_B}/\hbar$. $\Phi_B = \Phi_0 - \Phi_i$ is the barrier, where Φ_0 is the original trapezoidal barrier and Φ_i is the image potential. This expression indeed goes to $I \propto \exp(-2\kappa z_t)$ for $z_t \gg \kappa^{-1}$.

Next, we address the issue that the barrier including the image charge potential is not square, whereas Eq. (3) holds for a rectangular barrier. Reference 21 approximates the net barrier by a rectangular barrier with a height equal to the maximum of the net barrier. This is plotted as the dotted blue line in Fig. 3(b). In our work, we calculate the transmission for the real barrier using transfer matrices.[20] We start with a rectangular or trapezoidal barrier with height Φ_0 (here $\Phi_0 = 3.9$ eV). We then calculate the image potential for a certain z_t. We divide the net barrier into N square barriers, see inset II and III in Fig. 3(b). We typically use $N = 10^4$, as the results are converged at this value of N. Using the transfer matrices, we calculate the transmission and we repeat the procedure for all the tip-sample distances. We thus end up with the transmission versus z_t. Ideally, we want to fit these curves to the experimental $I(z_t)$ curves to find the original rectangular barrier Φ_0, because it allows us to extract the tip work function. In practice, this is nearly impossible due to the numerical calculations; thus, we reverse the method. We therefore extract the value of κ that an experimentalist would find from the calculated transmission curve. We do this by locally fitting the transmission curve with $\exp(-2\kappa_{app} z_t)$.[22] In Ref. 21, this is called the apparent barrier height or apparent decay length κ_{app}.

The barrier, including the image charges, goes to $-\infty$ at the edges. The image charge potential is a classical approach, and we are dealing with very short length scales in the angstrom regime. The WKB approach fails for rapidly varying potentials. Therefore, an atomistic view would be the proper

way to describe this problem, but in such an approach, it is nearly impossible to link an experimental decay length to a tip work function. Therefore, we stay in the classical approach, and we investigate two possibilities to deal with the singularities in the potential at the edges. The first is to fully include this in the transmission calculation. The result is the solid red line in Fig. 3(b). The second possibility is to include only the positive part of the barrier. The result of this approach is the long-dashed green line in Fig. 3(b).

We now discuss the summary given in Fig. 3(b) in more detail. The reduction in the barrier due to the image charges is shown by the dashed-dotted black line and the short-dashed cyan line. These are lines resulting from the simple calculation, neglecting all above described difficulties: $\kappa=\sqrt{2m_0\Phi_{B,\max}}/\hbar$. The dotted blue line is the approximation as described in Ref. 21. The barrier is approximated by a rectangular barrier, with a reduced height due to the image charges. The last two lines, the solid red line and the long dashed green line, result from the full transmission calculation for the image potential. For the red line, the negative part of the barrier is included, whereas we only include the positive part for the long-dashed green line. The calculations for these two lines include the most effects and will thus be the closest to reality. Please note that the exact shape of the solid red, dotted blue, and long-dashed green lines depend on the values of $\tilde{k}_t$ and $\tilde{k}_s$, which are not very well known. They depend on the kinetic energies and on the effective masses of the electron in the tip and the sample, especially the kinetic energy and the effective mass in the tungsten tip are relatively unknown. In the example shown here, we use $\tilde{k}_t=0.5$ Å^{-1} and $\tilde{k}_s=0.6$ Å^{-1}.

Figure 4 compares simulated κ versus z_t curves where we varied the parameters. We show the result for the transfer matrix method, where the negative part of the barrier is included [solid red line, Fig. 3(b), subset II] and where this part is neglected [long-dashed green line, Fig. 3(b), subset III]. The dashed-dotted black line corresponds to the original rectangular barrier. The left column displays the results for $\tilde{k}_t=0.01$ Å^{-1} and the right column for $\tilde{k}_t=0.5$ Å^{-1}. The rows correspond to different sample voltages as indicated. The main difference between the voltages is the wave vector in the sample, which is given by $\tilde{k}_s=\sqrt{2m_0m^{\star}E_{\text{kin}}}/(\hbar m^{\star})$. For 2 V, the electron tunnels into the CB, so the CB effective mass has to be used. The kinetic energy is given by the difference between the Fermi level of the tip and the onset of the CB, which is 0.5 eV for a sample voltage of 2 V. This gives $\tilde{k}_s=1.39$ Å^{-1}. For a positive voltage close to the conduction band, the kinetic energy is much smaller, 0.1 eV for a sample voltage of 1.6 V, leading to $\tilde{k}_s=0.62$ Å^{-1}. At negative voltages, the VB effective mass has to be used and the kinetic energy is given by the full VB of 6.5 eV.[23,24] This leads to $\tilde{k}_s=1.94$ Å^{-1}. We see that for large positive and negative voltages, the behavior is the same: κ drops for small z_t and there is a plateau for large z_t. The influence of the choice of $\tilde{k}_t$ is small. However, for small positive voltages,

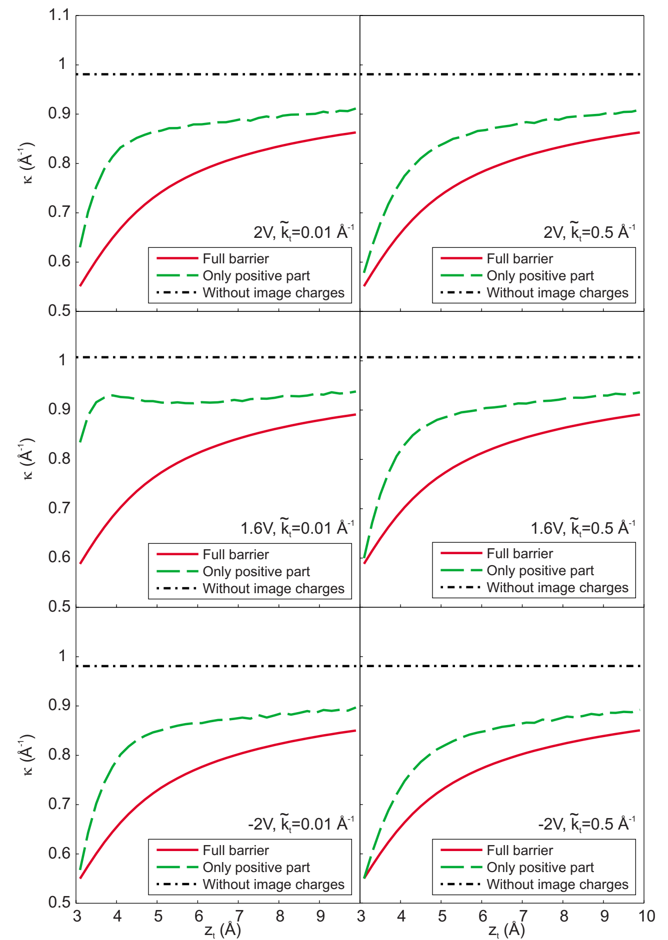

FIG. 4. (Color online) Simulated κ versus z_t curves for 2, 1.6, and −2 V for a tip work function of 3.9 eV. For the column, we used $\tilde{k}_t=0.01$ Å^{-1}, and for the right column $\tilde{k}_t=0.5$ Å^{-1}. We show both the curve as found when including the negative part of the potential (solid red line) and for the case that the negative part is neglected (long-dashed green line).

close to the onset of the CB, the choice of $\tilde{k}_t$ is significant and depending on this choice, there is a local maximum in the long-dashed green curve.

If we now turn to our experimental $\kappa(z_t)$ data (Fig. 5), we find a qualitative agreement. Please note that the x-axis displays Δz_t, because we do not know the absolute tip-sample distance. It is clear that the image charges play a role in the experiments; κ drops for small z_t, whereas for large z_t, there is a plateau, both in the experiment and in the simulations. The local maximum as was found in the simulations is also visible in the experiment. However, in this example, this local maximum is observed at a higher voltage than in the simulation. We neglected the effect of TIBB in the simulations. An upward TIBB at $V>0$ causes a reduced kinetic energy in the sample, which has the same effect as reducing the voltage in the simulation. Our data consisting of ~50 sets of κ vs z_t confirm the trend in the simulations, i.e., there is only a clear local maxima at relatively small positive voltages.

In the simulations, the plateau is detached from the dashed-dotted black line by ~10%, which leads to an under-

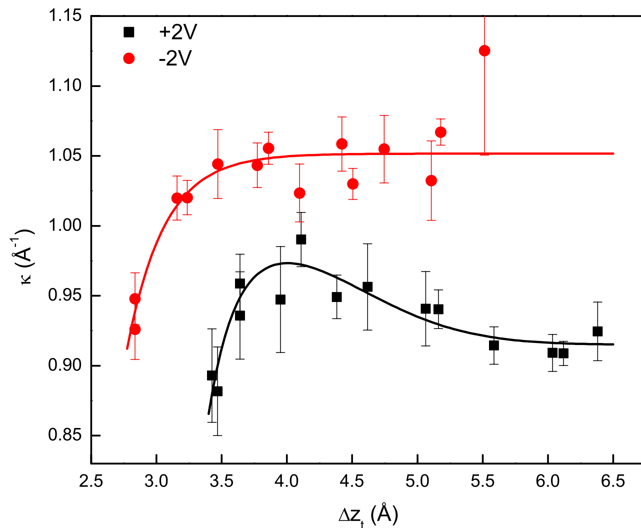

FIG. 5. (Color online) Comparison of a $\kappa(z_t)$ measurement at positive (red) and negative (black) voltages. Both measurements are done with the same tip at the same area of the sample.

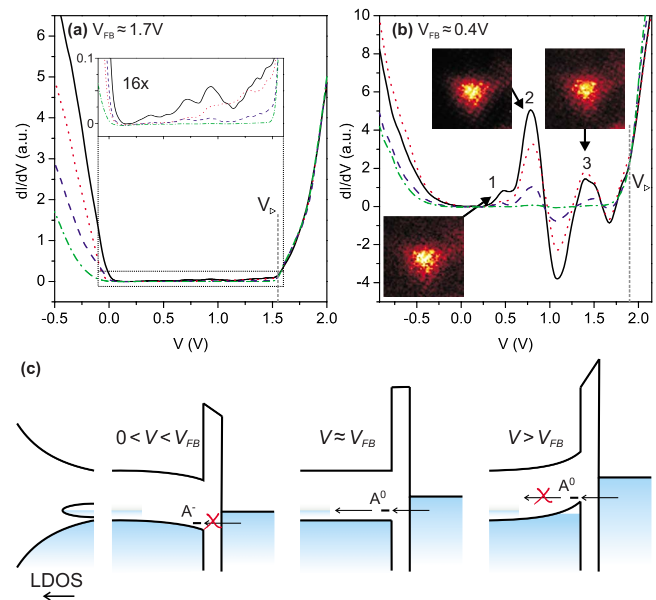

FIG. 6. (Color online) (a) and (b) dI/dV spectra on top of zinc atoms in various layers below the surface. $V_{\triangleright}$ is indicated. The inset in (b) shows the lateral contrast at the peak maxima. (c) Schematic of our model. The peaks in the dI/dV spectra occur around flatband, when the acceptor level close to the surface is aligned with the empty part of the impurity band in the bulk.

estimation of κ. We therefore correct the plateau value by 10% to obtain an optimal estimate for κ belonging to the original barrier. We realize that this is far from perfect, and we have to be careful about the absolute values for the tip work function and flatband voltage that we obtain. However, as long as we compare measurements where the tip work function is measured at the same voltage, we can compare the *relative* positions of the flatband voltage without any problems. We find a flatband condition of 1.7 V (Φ_{tip} =3.9 eV) for Figs. 1(a)–1(c) and 0.4 V (Φ_{tip}=5.5 eV) for Figs. 1(d) and 1(e). The large difference in tip work functions might seem surprising, because the tip work function is usually assumed to be around 4.5 eV for tungsten in STM studies. However, large variations are also reported in Ref. 25 for different crystal orientations. They find values ranging from 4.30 eV for the (116) plane to 5.99 eV for the (011) plane. They furthermore report that the work function depends on the annealing temperature, which is linked to the pureness of the crystal. They find a reduction of a few hundred meV for less pure crystals. Other studies show that the work function depends on the surface roughness.[26] They find a reduction of 0.6 eV when W is adsorbed on a (110) W single crystal for coverages below one monolayer. That means that we expect work functions ranging from 3.5 to 6 eV, which nicely corresponds to our measurements. This is an important indication that our method of extracting the tip work function is reliable.

V. ANALYSES AND INTERPRETATION

Returning to our observation of different $V_{\triangleright}$ for different tips, we come to the following conclusion. Tips with a high flatband condition, corresponding to a small tip work function, have a low $V_{\triangleright}$, whereas tips with low flatband condition, and thus a large tip work function, have a high $V_{\triangleright}$. This is indicated in Fig. 1.

In order to investigate this further, we measure dI/dV maps. At every pixel, we take an $I(V)$ spectrum, and afterward we take the numerical derivative. We eliminate crosstalk with the topography by choosing a setpoint where the contrast in the topography is vanishing. We measured dI/dV maps at the same areas of the sample and with the same tips as the topography images shown in Fig. 1. We can thus directly compare the topography images with the spectroscopy data and, furthermore, know the relative flatband conditions. Figures 6(a) and 6(b) show the dI/dV spectra. Figure 6(a) [Fig. 6(b)] is measured with the same tip as the measurements in Figs. 1(a)–1(c) [Figs. 1(d) and 1(e)]. In both graphs, the solid black curve is a spectrum on top of a Zn-atom very close to the surface (~layer 2), the dotted red line on top of a Zn-atom a bit deeper below the surface (~layer 5), and the dashed blue line on top of a Zn-atom very deep below the surface (~layer 8). The dashed-dotted green curve is on the bare surface. The two graphs are very different; in Fig. 6(a) there are hardly any peaks visible in the band gap, whereas in Fig. 6(b), very strong peaks followed by negative differential conductivity (NDC) are visible. The zoom shown in the inset of Fig. 6(a) shows some very weak peaks, but the NDC is absent.

Let us first explain the presence of the strong peaks in Fig. 6(b) and afterward explain their absence in Fig. 6(a). Our explanation differs from the interpretation in Ref. 8. This difference originates from the inclusion of image charges while extracting the flatband voltage, which shifts the flatband condition to lower voltages by ~1 V. Therefore, our model is based on upward TIBB, whereas Loth *et al.* assume downward TIBB. We propose a mechanism as shown in Fig. 6(c). The presence of the strong peaks indicates that we

have a very efficient tunneling path and the presence of NDC indicates that this tunneling path only exists in a small voltage window. There are two requirements for an efficient tunneling process at $V>0$ V. First, the acceptor level should be neutral (A^0), and second, the electron should be able to tunnel away from the acceptor into the bulk of the sample. The handle is the tip induced band bending,[16,27–30] which shifts the acceptor level with respect to the bulk VB. The TIBB depends on the applied voltage relative to the flatband (FB) voltage V_{FB}. For $V>V_{FB}$, the bands bend upward and the acceptor is neutral (A^0). For $V<V_{FB}$, the bands bend downward and the acceptor is negatively charged (A^-). In order to meet the first requirement, we need to apply a voltage above the flatband voltage. The second requirement is met when the acceptor level is aligned with the acceptor band in the bulk, which occurs around flatband. The samples are highly doped (2×10^{19} cm^{-3}), and therefore, there will be an acceptor band with a width of $\sim$30 meV.[31] This band will be partially filled, so there are empty states available in the bulk, slightly above the onset of the VB. This means that we have an energy window around flatband, where the tunneling is very efficient: at voltages below flatband, the acceptor is filled preventing efficient tunneling, and at voltages above flatband, the acceptor level is lifted above the empty acceptor band, and therefore, the electron cannot leave the Zn acceptor elastically. This immediately explains the presence of the negative differential conductivity: by increasing the voltage, the efficient tunneling channel via the Zn impurity disappears.

We now return to the absence of the peaks in Fig. 6(a). The difference in the two graphs is the tip work function and thus the flatband voltage. The flatband voltage is $\sim$1.7 and $\sim$0.4 V for Figs. 6(a) and 6(b), respectively. We therefore expect the first peak in Fig. 6(a) at an $\sim$1.3 V higher voltage than the first peak in Fig. 6(b). This corresponds to an external voltage of $\sim$2 V, which is at the edge of the spectrum, where the signal is dominated by tunneling into the conduction band.

Finally, we address the observation of more than one peak. Subtracting a reference spectrum measured on the bare surface from the spectra on top of the Zn atoms reveals a fourth peak, as is shown in Fig. 7. The presence of four peaks implies that the acceptor level is split into (at least) four levels. A similar splitting is observed for manganese in GaAs (Ref. 14) and manganese in InAs,[11] where three peaks were observed in both cases. For Mn in InAs, the three peaks are interpreted as different spin states, where the splitting from the $J=1$ ground state is due to spin orbit interaction,[11] whereas the splitting is smaller for Mn in GaAs, and was therefore attributed to the three projections of the $J=1$ ground state, which are split due to strain near the surface.[14] Atomic zinc has a $3d^{10}4s^2$ configuration, which carries no spin. However, the hole has a spin of $\frac{3}{2}$, which has four projections. These states can split, for example, due to strain present near the surface[9,14] or the electric field due to the

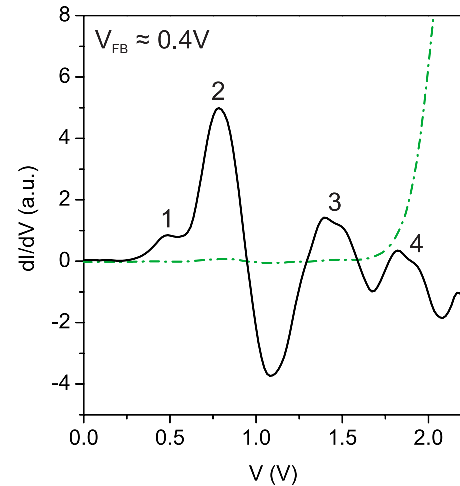

FIG. 7. (Color online) Subtracting a spectrum on the bare surface (dash-dotted green line) from a spectrum on top of a zinc atom reveals a forth peak (solid black line).

STM tip. It is surprising that all peaks have a similar lateral contrast [see inset in Fig. 6(b)]. However, this is also the case for Mn–GaAs.

We return to the observation that the triangles appear at very different voltages in the topography images for different tips. Tips with a high flatband condition [Figs. 1(a)–1(c) and Fig. 6(a)] have hardly any dI/dV peaks in the band gap, and in the topography images, a very low voltage has to be applied in order to see the triangles ($V_{\triangleright}=1.55$ V). This also coincides with the onset of the conduction band; the onset of the conduction band in Fig. 6(a) is $\sim$1.5 V. Tips with a low flatband condition [Figs. 1(d), 1(e), and 6(b)] have strong dI/dV peaks in the band gap, and in the topography images, the triangles already appear at a high voltage ($V_{\triangleright}=1.9$ V). This is slightly above the onset of the CB, but very close. This suggests that the triangles appear at a voltage where tunneling into the CB is mainly suppressed, as is indicated in Figs. 6(a) and 6(b).

VI. SUMMARY

In summary, we have investigated the effect of the tip work function in STM and STS. We have analyzed in detail the effect of image charges on the tunneling barrier in STM, including the effect of image charges, which causes a shift of the flatband condition to lower voltages by $\sim$1 V compared to the method proposed in Ref. 7. The range of tip work functions that we find corresponds to the expected range, indicating that our method of extracting the tip work function is reliable. This difference of $\sim$1 V in the flatband voltage leads to a different model to explain the negative differential conductivity. According to our model, the peaks in the dI/dV spectra occur when the acceptor level aligns with the empty part of the impurity band in the bulk, indicating that the wave function is imaged. The presence of four peaks suggests splitting of the acceptor level. The onset of the CB as found in the STS data coincides with the voltage where the

triangles appear in the topography images. This confirms the idea that the triangles appear when tunneling into the CB is suppressed.

ACKNOWLEDGMENTS

The authors thank Mervyn Roy, Peter Maksym, Karen Teichmann, Martin Wenderoth, and Sebastian Loth for the valuable discussions, and NAMASTE, COBRA, and STW-VICI Grant No. 6631 for financial support.

[1] J. F. Zheng, M. B. Salmeron, and E. R. Weber, Appl. Phys. Lett. **64**, 1836 (1994).
[2] Z. F. Zheng, M. B. Salmeron, and E. R. Weber, Appl. Phys. Lett. **65**, 790 (1994).
[3] A. M. Yakunin, A. Yu. Silov, P. M. Koenraad, J. H. Wolter, W. Van Roy, J. De Boeck, J.-M. Tang, and M. E. Flatté, Phys. Rev. Lett. **92**, 216806 (2004).
[4] R. de Kort, W. Kets, and H. van Kempen, Surf. Sci. **482–485**, 495 (2001).
[5] R. de Kort, M. C. M. M. van der Wielen, W. Kets, and H. van Kempen, Phys. Rev. B **63**, 125336 (2001).
[6] S. Loth, M. Wenderoth, R. G. Ulbrich, S. Malzer, and G. H. Döhler, Phys. Rev. B **76**, 235318 (2007).
[7] S. Loth, M. Wenderoth, and R. G. Ulbrich, Phys. Rev. B **77**, 115344 (2008).
[8] S. Loth, M. Wenderoth, R. G. Ulbrich, S. Malzer, and G. H. Döhler, Phys. Rev. Lett. **96**, 066403 (2006).
[9] C. Çelebi, J. K. Garleff, A. Yu. Silov, A. M. Yakunin, P. M. Koenraad, W. Van Roy, J.-M. Tang, and M. E. Flatté, Phys. Rev. Lett. **104**, 086404 (2010).
[10] J. K. Garleff, C. Çelebi, W. Van Roy, J.-M. Tang, M. E. Flatté, and P. M. Koenraad, Phys. Rev. B **78**, 075313 (2008).
[11] F. Marczinowski, J. Wiebe, J.-M. Tang, M. E. Flatté, M. Morgenstern, and R. Wiesendanger, Phys. Rev. Lett. **99**, 157202 (2007).
[12] G. Mahieu, B. Grandidier, D. Deresmes, J. P. Nys, D. Stiévenard, and Ph. Ebert, Phys. Rev. Lett. **94**, 026407 (2005).
[13] C. Çelebi, P. M. Koenraad, A. Yu. Silov, W. Van Roy, A. M. Monakhov, J.-M. Tang, and M. E. Flatté, Phys. Rev. B **77**, 075328 (2008).
[14] J. K. Garleff A. P. Wijnheijmer, A. Yu. Silov, J. van Bree, W. Van Roy, J.-M. Tang, M. E. Flatté, and P. M. Koenraad, Phys. Rev. B **82**, 035303 (2010).
[15] J. K. Garleff, M. Wenderoth, K. Sauthoff, R. G. Ulbrich, and M. Rohlfing, Phys. Rev. B **70**, 245424 (2004).
[16] R. M. Feenstra, J. Vac. Sci. Technol. B **21**, 2080 (2003).
[17] J. D. Jackson, *Classical Electrodynamics* (Wiley, New York, 1999), 3rd Ed., Chap. 2, 154–157.
[18] J. G. Simmons, J. Appl. Phys. **34**, 1793 (1963).
[19] J. Cazaux, Semicond. Sci. Technol. **13**, 827 (1998).
[20] J. H. Davies, *The Physics of Low-Dimensional Semiconductors, An Introduction*, (Cambridge University Press, Cambridge, England, 1998), Chaps. 5 and 7, 150–158 and 263–267.
[21] C. J. Chen, *Introduction to Scanning Tunneling Microscopy* (Oxford University Press, Oxford, 1993), Sec. 2.4.1, 62–63.
[22] We used $\kappa_{app} = -(1/2)(d/dz_t)(\ln(I(z_t)))$, instead of actually fitting the curve. For more details, see, for example, Ref. 21.
[23] J. R. Chelikowsky and M. L. Cohen, Phys. Rev. B **20**, 4150 (1979).
[24] J. R. Chelikowsky and M. L. Cohen, Solid State Commun. **29**, 267 (1979).
[25] E. W. Müller, J. Appl. Phys. **26**, 732 (1955).
[26] K. Besocke and H. Wagner, Phys. Rev. B **8**, 4597 (1973).
[27] R. M. Feenstra and J. A. Stroscio, J. Vac. Sci. Technol. B **5**, 923 (1987).
[28] K. Teichmann, M. Wenderoth, S. Loth, R. G. Ulbrich, J. K. Garleff, A. P. Wijnheijmer, and P. M. Koenraad, Phys. Rev. Lett. **101**, 076103 (2008).
[29] F. Marczinowski, J. Wiebe, F. Meier, K. Hashimoto, and R. Wiesendanger, Phys. Rev. B **77**, 115318 (2008).
[30] A. P. Wijnheijmer, J. K. Garleff, K. Teichmann, M. Wenderoth, S. Loth, R. G. Ulbrich, P. A. Maksym, M. Roy, and P. M. Koenraad, Phys. Rev. Lett. **102**, 166101 (2009).
[31] E. F. Schubert, *Doping in III-V Semiconductors* (Cambridge University Press, Cambridge, England, 1993), Section 1.3.3, 41–44.